

Triplet-Based Wireless Channel Charting

Paul Ferrand, Alexis Decurninge, Luis G. Ordoñez, Maxime Guillaud
Huawei Technologies

Abstract—Channel charting is a data-driven baseband processing technique consisting in applying unsupervised machine learning techniques to channel state information (CSI), with the objective of reducing the dimension of the data and extracting the fundamental parameters governing the distribution of CSI samples observed by a given receiver. In this work, we focus on neural network-based approaches, and propose a new architecture based on triplets of samples. It allows to simultaneously learn a meaningful similarity metric between CSI samples, on the basis of proximity in their respective acquisition times, and to perform the sought dimensionality reduction. The proposed approach is evaluated on a dataset of measured massive MIMO CSI, and is shown to perform well in comparison to the state-of-the-art methods (UMAP, autoencoders and siamese networks). In particular, we show that the obtained chart representation is topologically close to the geographical user position, despite the fact that the charting approach is not supervised by any geographical data.

I. INTRODUCTION

Recent evolutions of wireless network standards have considered increasingly higher numbers of antennas on its access points or base stations (BS), increased the bandwidth used for communication, and developed fine-grained multiple access techniques to track and manage these resources [1]. This comes at the expense of increasing the number of parameters (known collectively as channel state information, or CSI) necessary to track the propagation channel in real-time by the BS for all users in the system.

However, for a given BS deployment and its environment, ray-tracing models have long validated that it is possible to associate a realistic wireless channel with a relatively smaller set of parameters, including in particular user position as well as other geometric features of the propagation environment [2]. Indeed, the set of *possible* channels that a user can experience, discounting ephemeral scatterers and shadow fades, is therefore primarily determined by its position in space. Learning a correspondence between CSI points belonging to a high-dimensional space (*ambient* space) and their representations belonging to low-dimensional space (*latent* space) could be then used to enhance numerous network functionalities, such as predictive radio resource management and rate adaptation, handover between cells, beam association and user tracking and pairing or grouping in Device-to-Device (D2D) scenarios. This fact is the implicit motivation behind the use of radio maps to evaluate and predict the channel quality of users depending on their position in space [3], [4], and is at the heart of the channel charting framework developed by Studer *et al.* in [5], where the user’s absolute position is replaced by a pseudo-position on a chart.

Channel charting applies classical unsupervised dimensionality reduction methods from machine learning (see e.g. [6] or [7] for an overview of dimensionality reduction methods) to CSI data. Based on a large dataset of CSI samples acquired in a given environment, it maps each CSI sample onto a corresponding point in a latent space, called *chart*, in an unsupervised manner, while preserving relative sample distances between the CSI space and the latent space. Due to its unsupervised nature, channel charting is applicable without any need of the user location nor of a faithful geometric model of the user’s environment. As such, the chart is an attempt to identify a set of essential parameters capturing the information contained on the CSI. In [5] and subsequent work [8]–[10], the authors have studied different approaches to learn the channel chart based on simulated CSI data, centered around Sammon’s mapping, autoencoders, and the so-called Siamese networks.

Textbook dimensionality reduction algorithms aim to optimize a cost function involving distances in both the ambient space and the latent space. It is however difficult to define a meaningful distance between two CSI samples in the ambient space. In order to address this shortcoming, channel moments of order 2 were used as features in [5], and a sparse representation of the channel impulse response in the spatial and temporal domain was used as a set of features [8]. Conversely, in this paper we propose to learn the charting function based on neighborhood (or class) knowledge in the ambient space only, without requiring a quantitative distance measure, by merely training a neural network to discriminate between “close” data points and “far” data points. The high-dimensional distance can then be deduced as the distance between low-dimensional points seen through the learned charting function. This technique has been studied in the 2000s, most particularly in classical works on metric learning [11], [12]. The problem considered was based on the Mahalanobis distance between samples selected as a *triplet*, where 2 elements of the triplets belonged to the same class, while the last element was an outsider. More recently, a similar approach has been proposed for face classification under the name “FaceNet” [13] using a similar triplet construction.

The paper is organized as follows. We first introduce the general framework of dimensionality reduction in Section II before relaxing the need for distances in the ambient space in Section III. We then detail the simulated algorithms in Section IV and compare their results in Section V both qualitatively and quantitatively.

II. DIMENSIONALITY REDUCTION

Let us consider a random variable X of unknown distribution with values in $\mathcal{X} \subset \mathbb{C}^D$. Assume that N samples from X are available and indexed by i , $1 \leq i \leq N$. Given another space $\mathcal{Y} \subset \mathbb{C}^d$ with $d \ll D$, the dimensionality reduction problem consists in assigning coordinates $\mathbf{y}_i \in \mathcal{Y}$ to the i -th sample, \mathbf{x}_i , such that

$$\|\mathbf{y}_i - \mathbf{y}_j\| \approx \|\mathbf{x}_i - \mathbf{x}_j\| \quad \text{for all } (i, j) \in \mathcal{S} \quad (1)$$

where $\|\cdot\|$ denotes the Euclidean norm¹ on \mathbb{R}^D or \mathbb{R}^d (the approximation will be made rigorous later) and \mathcal{S} denotes some set of sample indices pairs. For instance, taking $\mathcal{S} = \llbracket 1 \dots N \rrbracket \times \llbracket 1 \dots N \rrbracket$ yields the classical multi-dimensional scaling (MDS) approach [14], while taking \mathcal{S} as the set indices pairs (i, j) such that \mathbf{x}_i and \mathbf{x}_j are neighbors in \mathcal{X} (i.e. $\|\mathbf{x}_i - \mathbf{x}_j\|$ is below a certain threshold) is the starting point of the ISOMAP algorithm [15]. Sammon's mapping [16] consists in weighting the importance of the constraint in (1) with a factor monotonically decreasing in $\|\mathbf{x}_i - \mathbf{x}_j\|$.

Of particular interest is the case where there exists a generative model such that X arises from a d -dimensional random variable W with values in $\mathcal{W} \subset \mathbb{R}^d$ via a smooth bijective mapping $g : \mathcal{W} \rightarrow \mathcal{X}$, i.e.,

$$\mathbf{x}_i = g(\mathbf{w}_i) \quad (2)$$

where \mathbf{w}_i is sampled from W . In that case, $g(\mathcal{W})$ can be seen as a manifold embedded in \mathbb{R}^D , and \mathcal{X} is a manifold-valued random variable. If we knew this mapping, we could choose $\mathbf{y}_i = g^{-1}(\mathbf{x}_i) = \mathbf{w}_i$, which fulfills (1) with equality. In the case of interest, where dimensionality reduction is applied to CSI samples, W can be thought of as the parameters of the Maxwell equations that govern propagation, while X is the channel state, and \mathcal{Y} is the channel chart.

In general, the generative model (function g and the \mathbf{w}_i) is unknown, and we have only access to the observations \mathbf{x}_i . Therefore, we need to infer a smooth mapping $f : \mathcal{X} \rightarrow \mathcal{Y}$ such that the \mathbf{y}_i are given by $\mathbf{y}_i = f(\mathbf{x}_i)$ which enforces the distance preservation property, i.e., for all i, j , it holds $\|f(\mathbf{x}_i) - f(\mathbf{x}_j)\| \approx \|\mathbf{x}_i - \mathbf{x}_j\|$. The situation can be summarized as follows:

$$\underbrace{\mathcal{W} \subset \mathbb{R}^d \xrightarrow{g} \mathbf{w}_i}_{\text{Generative model}} \quad \underbrace{\mathcal{X} \subset \mathbb{R}^D \xrightarrow{f} \mathbf{x}_i}_{\text{Observations}} \quad \underbrace{\mathcal{Y} \subset \mathbb{R}^d \xrightarrow{f} \mathbf{y}_i}_{\text{Dimensionality Reduction}} \quad (3)$$

Henceforth, we focus on the case where f is a parametric function defined by a deep neural network (DNN), trained to optimize some objective function guaranteeing (1) over a set of training samples. For instance, letting θ denote the parameters of the DNN and f_θ its transfer function, we let $f = f_{\theta^*}$ where

$$\theta^* = \arg \min_{\theta} \sum_{i,j \in \mathcal{S}} (\|f_\theta(\mathbf{x}_i) - f_\theta(\mathbf{x}_j)\| - \|\mathbf{x}_i - \mathbf{x}_j\|)^2. \quad (4)$$

The DNN-based parametric approach ($\mathbf{y}_i = f_\theta(\mathbf{x}_i)$) has a significant advantage over other dimensionality reduction

approaches: it handles gracefully the so-called *out-of-sample extension* problem, i.e., the chart coordinates for a new sample \mathbf{x} not present in the training dataset can be computed directly by evaluating $f_{\theta^*}(\mathbf{x})$; while spectral methods such as ISOMAP, which consist in computing the coordinates \mathbf{y}_i for each i in the dataset, would require to solve the whole problem again or apply barycentric methods, usually at much higher computational cost [17].

In practical applications of dimensionality reduction to CSI data, we additionally face the following practical issues:

- The problem can only be solved up to an isometric transformation in \mathcal{Y} , since it is entirely defined by distance constraints (1).
- Only a noisy version of \mathbf{x}_i can be observed.
- Since dimension d is not known, the problem is generally formulated based on a heuristic choice of the dimension of \mathcal{Y} .

III. RELAXING THE NEED FOR DISTANCES IN THE AMBIENT SPACE

Another difficulty in applying dimensionality reduction to CSI data is the fact that the Euclidean distance between two CSI samples is usually a poor measure of similarity as understood by physical layer communications engineers. In particular, identical or similar propagation conditions might yield CSI samples with high Euclidean distance because the samples are subject to random impairments such as (real) scaling resulting from different transmission power or automatic gain control, complex phases (possibly frequency-dependent) stemming from timing or clock frequency offsets, or RF chain calibration. Since the Euclidean distance in \mathcal{X} is not meaningful, we have to resort to distance learning [11] as an alternative way to define the distance between CSI samples.

In a cellular system, CSI is typically estimated at a rate of several dozens or hundreds times per second. Depending on the mobile device velocity, the distance in space between the locations corresponding to consecutive CSI samples is well within the channel coherence distance (usually assumed to be commensurate with the wavelength). For $i \in \mathcal{S}$, let t_i denote the absolute time of acquisition of \mathbf{x}_i . We propose to use the time difference between samples, $|t_i - t_j|$ for samples i and j , as a proxy to infer a meaningful distance.

More specifically, given a triplet of samples $(\mathbf{x}_i, \mathbf{x}_j, \mathbf{x}_k) \in \mathcal{T}_T \subset \mathcal{S}^3$ acquired at absolute times t_i, t_j, t_k respectively, and for a small constant T (say, $T = .2s$) such that $|t_j - t_i| \leq T \leq |t_k - t_i|$, we can implicitly define a distance d_{CSI} on \mathcal{X} by noting that it should fulfill

$$d_{\text{CSI}}(\mathbf{x}_i, \mathbf{x}_j) \leq d_{\text{CSI}}(\mathbf{x}_i, \mathbf{x}_k) \quad (5)$$

with high probability. In this context, the reference sample \mathbf{x}_i is called the anchor. Using again the DNN-based parametric architecture, and defining the distance as $d_{\text{CSI}}(\mathbf{x}, \mathbf{x}') =$

¹We will relax the Euclidean norm assumption hereafter.

$\|f_{\theta}(x) - f_{\theta}(x')\|$, we can infer f_{θ} by optimization over θ of a cost function that penalizes the violations of (5), i.e.

$$\theta^* = \arg \min_{\theta} \sum_{(i,j,k) \in \mathcal{T}_T} \left(\|f_{\theta}(x_j) - f_{\theta}(x_i)\| - \|f_{\theta}(x_k) - f_{\theta}(x_i)\| \right)^+ . \quad (6)$$

IV. CONSIDERED DNN TRAINING ARCHITECTURES

Among the channel charting approaches considered in the literature, autoencoders [10] and Siamese networks [9] have received particular attention. Let us first describe these classical designs, and then show how our proposed architecture departs from them.

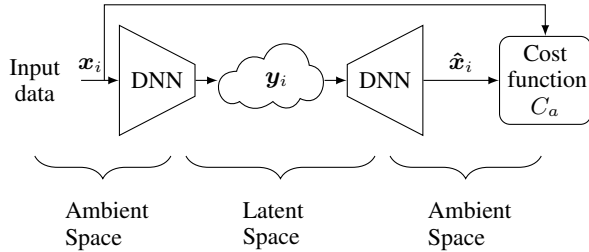


Fig. 1: Structure of a generic autoencoder.

Fig. 1 depicts a generic autoencoder such as the one studied in [10]. A first DNN processes the input data from the ambient space to the latent space, i.e., mapping a sample x_i to $y_i = f_{\theta^*}(x_i)$. Then, a second DNN takes the data from the latent space back to the ambient space \hat{x}_i . Typically, the cost function associated with an autoencoder is based on the distance between the input and the output:

$$C_a \equiv \frac{1}{N} \sum_i \|x_i - \hat{x}_i\|. \quad (7)$$

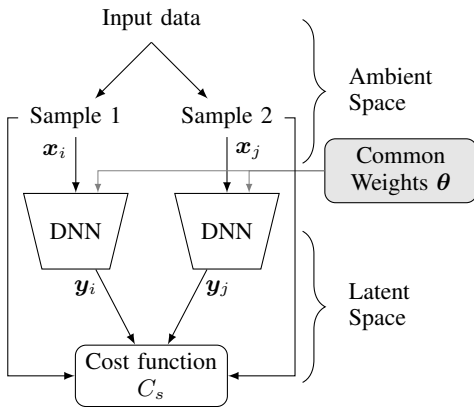


Fig. 2: Structure of a generic Siamese networks architecture. Both DNN block are identical, and use the same weights.

Fig. 2 depicts a generic Siamese network architecture as studied in [9] that also uses an unspecified deep neural network (DNN) block to process a pair of input samples x_i and x_j . Both samples produce a representation in the latent space

y_i and y_j . The Siamese network is then trained to try and replicate the ambient space distance between the samples in the latent space, i.e. minimizing

$$C_s \equiv \frac{1}{N} \sum_i (\|x_i - x_j\| - d_{\text{CSI}}(x_i, x_j))^2 \quad (8)$$

with $d_{\text{CSI}}(x_i, x_j) = \|y_j - y_i\|$.

Observe at this point that both cost functions (7) and (8) involve distances in the ambient space, i.e., distances between the input samples x_i . As discussed earlier, we would prefer to actively avoid distances in this space. Hence, we propose to merge the dimensionality reduction with the distance learning approach outlined in Section III so that we focus only on distances in the latent space.

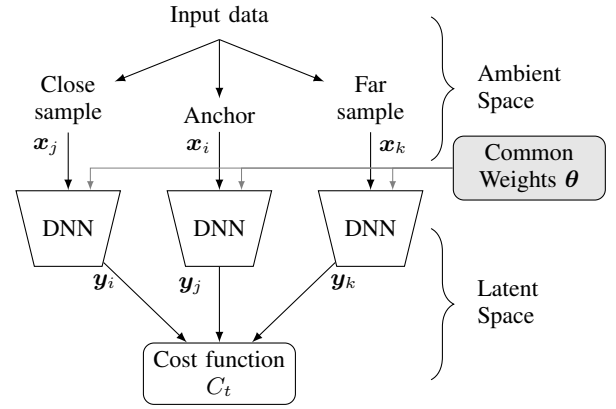


Fig. 3: Triplet network architecture as introduced in [13] as “FaceNet”. The three DNN blocks are identical, and use common weights.

Letting $d_{\text{CSI}}(x_i, x_j)$ and $d_{\text{CSI}}(x_i, x_k)$ denote the distances between the anchor and the “close” and “far” samples, respectively, the cost function in (6) can be optimized through the triplet network architecture depicted in Fig. 3 where the cost function C_t is chosen as

$$\frac{1}{N} \sum_{(i,j,k) \in \mathcal{T}_T} (d_{\text{CSI}}(x_i, x_j) - d_{\text{CSI}}(x_i, x_k) + M)^+, \quad (9)$$

and where M is a margin that can be set to 1 without loss of generality since the embedding is scale-independent in this context. Alternatively, we propose to also consider here a log-sum-exp cost function C_t as

$$\log \left(\sum_{(i,j,k) \in \mathcal{T}_T} \exp [d_{\text{CSI}}(x_i, x_j) - d_{\text{CSI}}(x_i, x_k)] \right). \quad (10)$$

While the cost functions in (9) and (10) appear to be parameter-less, there are somewhat hidden meta-parameters in triplet networks, as one has to build triplets in order to favor learning the embedding and spanning the whole set of \mathcal{T}_T in practice is impractical. Intuitively, the choice of triplets is as important as the actual objective function or the method used to learn the embedding; since there is no *a priori* representative

distribution of the triplets, the construction of the training batches will strongly influence the resulting embedding. This particular fact was identified in [13], [18], where different ways to favor the accuracy and training speed of triplet-based approaches are proposed. Additionally, the selection of triplets can also be increasingly hardened so that the embedding discriminates better between the classes; such an approach is called *curriculum learning* or *shaping* [19].

V. EXPERIMENTAL RESULTS

In this section we compare the triplet approach to the earlier proposals in channel charting as well as an embedding generated by UMAP [6] from our training dataset.

A. Experimental data

We use experimental data gathered from a commercial cellular base station (BS) connected to a single user equipment (UE) for the charting training and testing sets. The BS is equipped with 64 antennas arranged regularly in a rectangular array of 4×8 and each antenna element has 2 polarizations. The BS collects samples at a frequency of 200 Hz, leading to a sampling period of 5 ms. Each sample consists in 288 frequency data points regularly separated over a 20 MHz bandwidth, together with a timestamp and Global Navigation Satellite System (GNSS) position for reference. We use i , f , n , m and p to index the time, frequency, vertical antenna, horizontal antenna, and polarization, so that each channel sample is denoted by $h_i(p, m, n, f)$.

In practical cellular systems, a number of hardware and protocol design characteristics might corrupt the wireless channel state as it is seen by the BS. Dominant impairments are usually related to:

- Manufacturing variations within the radio-frequency components connected to each antenna, which cause multiplicative impairments on each antenna port; such impairments are typically compensated up to a common complex phase shift which may change upon recalibration of the array.
- Clock and frequency offsets between the UE and the BS: although oscillators in such a system are expected to be synchronized, residual offsets and phase noise may have significant enough effects when considering long measurement periods; the effect is a linear (with time) phase shift.
- Timing advance variations at the BS: in the context of 4G and 5G cellular systems based on orthogonal frequency division multiple access (OFDMA), a *timing advance* mechanism allows the BS to command the UE to advance or delay its own clock in order to synchronize the reception of signals from several users at the BS.

Some feature engineering techniques have been proposed in [20] to alleviate these impairments, and we adopt here the same pre-processing, which can be summarized as follows:

- 1) Apply a 2D Fourier transform to the corrupted channel measurements $h_i(p, m, n, f)$ to form the beam domain

channel measurements $\tilde{h}_i(p, z, a, f)$ where z and a index the zenith and azimuth beam respectively. Such a transformation has already been shown to help charting algorithms in [5].

- 2) Compute the absolute value of the frequency-domain complex autocorrelation $r_i(p, z, a, \delta)$, where δ denotes the autocorrelation lag in the frequency f dimension. We further downsample and truncate the autocorrelation in the δ dimension, to consider 16 elements from the first 64 lags.
- 3) Take the logarithm of the result, i.e. $\log |r_i(p, z, a, \delta)|$.

This feature design allows to work with features consisting of 1024 real coefficients at the input of the neural network (down from 18,432 complex coefficients in the raw samples), and more importantly removes certain impairments specific to CSI as estimated by the BS.

B. Basic deep neural network block

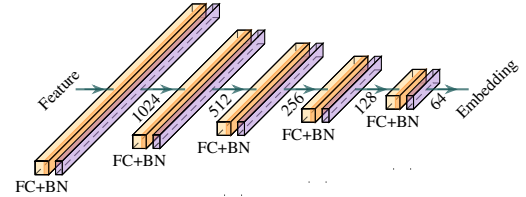


Fig. 4: Neural network composed of 5 fully connected (FC) layers and batch normalization (BN). Each fully connected layer except the last one apply a ReLU nonlinearity.

For all considered approaches, we use the DNN from [20] (depicted in Fig. 4) as a basic building block. The number of parameters in the model adds up to 1.7 million single precision floats. In all cases, we use a mean-squared loss and the Adam optimizer [21]. The total size of the training set was around 2.8 million samples (roughly 4 hours worth of data). The implementation relied on Tensorflow [22], trained each for 100 epochs and a batch size of 1000. For the Siamese and triplet approaches, we selected 2000 batches of size 1000.

C. Resulting embeddings

Let us first consider a latent space of dimension $d = 2$ for the sake of convenient graphical representation. The GNSS position is used as a reference to create 4 different classes (colored areas in Fig. 5a), and we check the ability of the obtained charts to reproduce this separation. The 2-dimensional representation of the channel charts obtained through different methods in Figs. 5b-5f. We clearly see in these representation that the triplets network manage to identify coarsely the underlying geometry of the data and reproduce the quadrants up to some deformation. Interestingly, the representation obtained by the Siamese architecture is very similar to that obtained through principal component decomposition of the features.

We now seek to numerically evaluate the quality of the charts by comparing the obtained latent space with a *reference* space, for which we use the GNSS position in order to

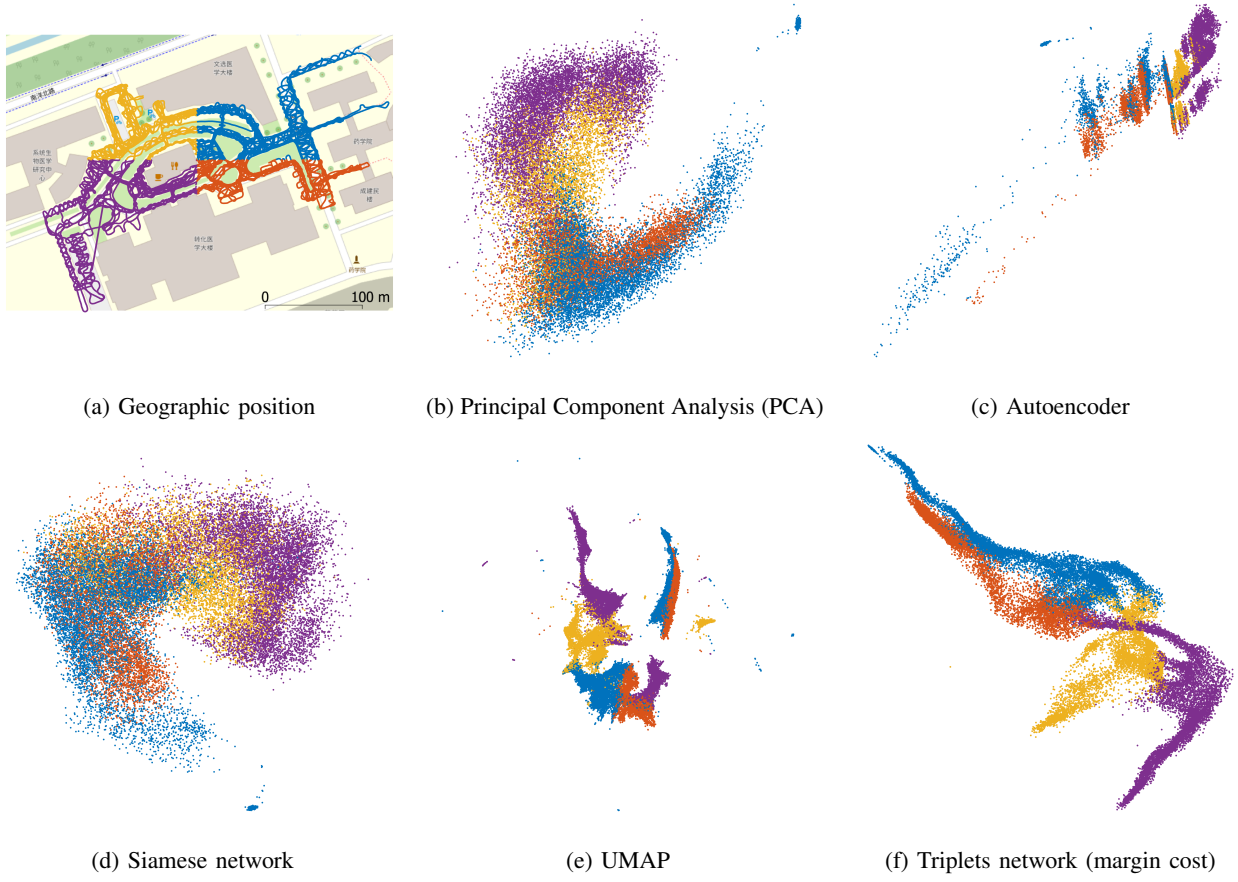


Fig. 5: Visual representation of the different channel charts obtained on the same training dataset. The colors are computed from the position to distinguish the 4 quadrants. The triplet network trained with the log-sum-exp cost has a similar shape to the one trained with the margin cost.

avoid the need to define distances in the ambient space. The typical metrics for this are the Kruskal stress [14] and the neighborhood-oriented trustworthiness and continuity [23]. Let $d_{i,j}$ be the geographical distance between points i and j , and $\hat{d}_{i,j}$ the distances in the latent space of the considered channel chart. The Kruskal stress is defined as follows:

$$KS = \sqrt{\frac{\sum_i \sum_j (d_{i,j} - \hat{d}_{i,j})^2}{\sum_i \sum_j d_{i,j}^2}}. \quad (11)$$

The lower the Kruskal stress, the closer the two spaces in terms of pairwise distances. Kruskal stress was originally designed as an optimization metric, and as such without additional constraint the global scale of the reference space and the latent space tended to be equal. Since we are using it as an evaluation metric after extracting the latent space, we need to rescale the latter to match the scale of the reference geographical space.

Trustworthiness seeks to penalize neighbors in the chart that are not neighbors in the reference space. Let $\hat{\mathcal{N}}_i^K$ be the set of K neighbors of the point indexed by t in the latent space, and let $r_i(u)$ be the rank of the point indexed by u among the neighbors of t in the reference space. The trustworthiness

(TW) is then defined as

$$TW = 1 - \frac{1}{NC} \sum_{i \in \mathcal{S}} \sum_{u \in \hat{\mathcal{N}}_i^K} (r_i(u) - K)^+ \quad (12)$$

where $C = K(2N - 3K - 1)/2$ is a normalization constant. The penalty $(r_i(u) - K)^+$ will be 0 if u is a K -neighbor of t in the reference space.

Continuity (CT) is a similarly defined metric, except that it penalizes points that are neighbors in the reference space but not in the latent space. In fact, CT can be obtained by swapping the reference and latent space in the definition of the trustworthiness. Let \mathcal{N}_i^K be the set of K neighbors of the point indexed by t in the reference space, and let $\hat{r}_i(u)$ be the rank of the point indexed by u among the neighbors of t in the latent space. Continuity is then defined as

$$CT = 1 - \frac{1}{NC} \sum_{i \in \mathcal{S}} \sum_{u \in \mathcal{N}_i^K} (\hat{r}_i(u) - K)^+. \quad (13)$$

Due to the large number of points in the considered dataset, the computation of CT and TW is itself computationally complex. Therefore, we resort to transforming the trustworthiness (12) and continuity (13) expressions into respective

Monte-Carlo versions. To do so, instead of considering the average over all indices i , we sample a subset $\mathcal{I} \subset \mathcal{S}$ and compute the trustworthiness as

$$\text{TW} \approx 1 - \frac{1}{|\mathcal{I}|C} \sum_{i \in \mathcal{I}} \sum_{u \in \tilde{\mathcal{N}}_i^K} (r_i(u) - K)^+ \quad (14)$$

where $|\mathcal{I}|$ is the cardinality of \mathcal{I} . The same procedure can be applied to the continuity.

We reproduce the results for our experiments in Tab. I. They demonstrate that the triplet with margin loss always outperforms the other considered approaches in terms of continuity and trustworthiness. In terms of Kruskal stress, the triplet approach with margin loss performs well for low target dimensions ($d = 2$), however it is outperformed by Siamese networks for higher dimensions.

VI. CONCLUSION

In this paper, we described a triplet-based approach for channel charting that can be leveraged on training datasets that are gathered consecutively over time. We use this time information to teach the network to discriminate between CSI points that are close, and points that are far, and use the learned distance to produce a representation of the points in a low-dimensional latent space. We evaluated the performance of this approach against the state of the art in channel charting and in dimensionality reduction approaches in general.

In further work, we will evaluate the use of the obtained channel charts in practical scenarios. We also plan to tune the evaluation metrics used to evaluate the different charting approaches up to now. As seen on Tab. I, when we increase the dimension of the latent space, it also becomes harder to discriminate between the different approaches. The insight provided by realistic applications could steer us in the right direction to build more precise metrics.

REFERENCES

- [1] E. G. Larsson, O. Edfors, F. Tufvesson, and T. L. Marzetta, “Massive MIMO for next generation wireless systems,” *IEEE Communications Magazine*, vol. 52, no. 2, pp. 186–195, 2014.

	TW	CT	Kruskal stress
PCA (dim. 2)	0.843	0.894	0.629
Siamese networks (dim. 2)	0.846	0.910	0.494
Autoencoders (dim. 2)	0.929	0.889	0.701
UMAP (dim. 2)	0.951	0.923	0.526
Triplets (exp. loss) (dim. 2)	0.957	0.975	0.238
Triplets (margin loss) (dim. 2)	0.967	0.977	0.206
Siamese network (dim. 5)	0.940	0.940	0.496
Autoencoders (dim. 5)	0.972	0.968	0.877
Triplets (exp. loss) (dim. 5)	0.969	0.974	0.767
Triplets (margin loss) (dim. 5)	0.973	0.976	0.500
Siamese network (dim. 10)	0.960	0.938	0.500
Autoencoders (dim. 10)	0.975	0.967	0.694
Triplets (exp. loss) (dim. 10)	0.978	0.976	0.850
Triplets (margin loss) (dim. 10)	0.979	0.976	0.723

TABLE I: Quality metrics computed on the charts.

- [2] P. Ferrand, M. Amara, S. Valentin, and M. Guillaud, “Trends and challenges in wireless channel modeling for evolving radio access,” *IEEE Communications Magazine*, vol. 54, no. 7, pp. 93–99, 2016.
- [3] R. Di Taranto, S. Muppirisetty, R. Raulefs, D. Slock, T. Svensson, and H. Wymeersch, “Location-aware communications for 5g networks: How location information can improve scalability, latency, and robustness of 5g,” *IEEE Signal Processing Magazine*, vol. 31, no. 6, pp. 102–112, 2014.
- [4] N. Bui, M. Cesana, S. A. Hosseini, Q. Liao, I. Malanchini, and J. Widmer, “A survey of anticipatory mobile networking: Context-based classification, prediction methodologies, and optimization techniques,” *IEEE Communications Surveys Tutorials*, vol. 19, no. 3, pp. 1790–1821, 2017.
- [5] C. Studer, S. Medjkouh, E. Gönültaş, T. Goldstein, and O. Tirkkonen, “Channel charting: Locating users within the radio environment using channel state information,” *IEEE Access*, vol. 6, pp. 47 682–47 698, 2018.
- [6] L. McInnes, J. Healy, and J. Melville, “UMAP: Uniform manifold approximation and projection for dimension reduction,” 2018. [Online]. Available: <https://arxiv.org/abs/1802.03426v2>
- [7] J. A. Lee and M. Verleysen, *Nonlinear Dimensionality Reduction*. Springer, 2007.
- [8] J. Deng, S. Medjkouh, N. Malm, O. Tirkkonen, and C. Studer, “Multi-point channel charting for wireless networks,” in *2018 52nd Asilomar Conference on Signals, Systems, and Computers*, 2018, pp. 286–290.
- [9] E. Lei, O. Castañeda, O. Tirkkonen, T. Goldstein, and C. Studer, “Siamese neural networks for wireless positioning and channel charting,” 2019.
- [10] P. Huang, O. Castañeda, E. Gönültaş, S. Medjkouh, O. Tirkkonen, T. Goldstein, and C. Studer, “Improving channel charting with representation-constrained autoencoders,” in *IEEE International Workshop on Signal Processing Advances in Wireless Communications (SPAWC)*, July 2019.
- [11] K. Q. Weinberger and L. K. Saul, “Distance metric learning for large margin nearest neighbor classification,” *Journal of Machine Learning Research*, no. 10, pp. 207–244, Feb. 2009.
- [12] C. Shen, J. Kim, L. Wang, and A. Hengel, “Positive semidefinite metric learning with boosting,” in *Proc. Advances in Neural Information Processing Systems*, 2009, pp. 1651–1659.
- [13] F. Schroff, D. Kalenichenko, and J. Philbin, “Facenet: A unified embedding for face recognition and clustering,” in *IEEE Conference on Computer Vision and Pattern Recognition (CVPR)*. IEEE, 2015, pp. 815–823.
- [14] J. B. Kruskal, “Multidimensional scaling by optimizing goodness of fit to a nonmetric hypothesis,” *Psychometrika*, vol. 29, no. 1, 1964.
- [15] J. B. Tenenbaum, V. de Silva, and J. C. Langford, “A global geometric framework for nonlinear dimensionality reduction,” *Science*, vol. 290, no. 12, pp. 2319–2323, 2000.
- [16] J. W. Sammon, “A nonlinear mapping for data structure analysis,” *IEEE Transactions on Computers*, vol. C-18, no. 5, pp. 401–409, 1969.
- [17] Y. Bengio, J.-F. Paiement, P. Vincent, O. Delalleau, N. L. Roux, and M. Ouimet, “Out-of-sample extensions for lle, isomap, mds, eigenmaps, and spectral clustering,” in *Proceedings of the 16th International Conference on Neural Information Processing Systems*, 2003, p. 177a–184.
- [18] A. Hermans, L. Beyer, and B. Leibe, “In Defense of the Triplet Loss for Person Re-Identification,” *arXiv:1703.07737 [cs]*, Nov. 2017, arXiv: 1703.07737. [Online]. Available: <http://arxiv.org/abs/1703.07737>
- [19] Y. Bengio, J. Louradour, R. Collobert, and J. Weston, “Curriculum learning,” in *Proceedings of the 26th International Conference on Machine Learning*, 2009.
- [20] P. Ferrand, A. Decurninge, and M. Guillaud, “DNN-based localization from channel estimates: Feature design and experimental results,” submitted to Globecom 2020. [Online]. Available: <https://arxiv.org/abs/2004.00363>
- [21] D. P. Kingma and J. Ba, “Adam: A method for stochastic optimization,” in *International Conference for Learning Representations*, 2015.
- [22] Abadi, M. et al., “TensorFlow: Large-scale machine learning on heterogeneous systems,” 2015. [Online]. Available: <https://www.tensorflow.org/>
- [23] J. Venna and S. Kaski, “Neighborhood preservation in nonlinear projection methods: An experimental study,” in *Lecture Notes in Computer Science*, vol. 2130, 09 2001.